Nonholonomic Virtual Constraints for Control of Powered Prostheses Across Walking Speeds

Jonathan C. Horn and Robert D. Gregg

***Abstract*—This paper presents a method to design a nonholonomic virtual constraint (NHVC) controller that produces multiple distinct stance-phase trajectories for corresponding walking speeds. NHVCs encode velocity-dependent joint trajectories via momenta conjugate to the unactuated degree(s)-of-freedom of the system. We recently introduced a method for designing NHVCs that allow for stable bipedal robotic walking across variable terrain slopes. This work extends the notion of NHVCs for application to variable-cadence powered prostheses. Using the segmental conjugate momentum for the prosthesis, an optimization problem is used to design a single stance-phase NHVC for three distinct walking speed trajectories (slow, normal, and fast). This stance-phase controller is implemented with a holonomic swing phase controller on a powered knee-ankle prosthesis, and experiments are conducted with an able-bodied user walking in steady and non-steady velocity conditions. The control scheme is capable of representing 1) multiple, task-dependent reference trajectories, and 2) walking gait variance due to both temporal and kinematic changes in user motion.**

***Index Terms*—Rehabilitation Robots, Underactuated Robots, Motion Control**

I. Introduction

Individuals with lower-limb amputation traditionally walk with passive prosthetic legs that dissipate energy and provide a sense of stability for the user. Although these passive devices enable locomotion, they do not restore the motor control and positive mechanical work necessary to perform various activities without significant compensations and effort from the user. The intact joint compensations involved in walking with passive prostheses [1] require higher metabolic cost than able-bodied locomotion and increase the risk for back pain and osteoarthritis [2]. Powered prostheses offer a potential solution to the shortcomings of traditional passive prostheses [3].

The goal of powered prostheses is typically to reproduce normative joint kinematics and kinetics for a variety of activities, because restoring biological leg biomechanics can in turn reduce the intact joint compensations associated with using a passive prosthesis [4]–[6]. Many different control strategies have been implemented on powered prostheses for this purpose. Impedance-based control schemes have successfully replicated nominal human walking for multiple locomotion tasks, and offer inherent stability between the human and prosthetic device due to the passive nature of the closed-loop dynamics [7]–[12]. Despite the advantages of impedance-based strategies, one shortcoming is the excessive amount of control parameters that require tuning for every user [13], [14]. Techniques are being developed to automate the configuration of these controllers [15], [16], but these procedures remain time intensive and limited in the number of joints and parameters that can be simultaneously tuned. Another method that has garnered recent attention is virtual constraint-based control. Virtual holonomic constraints (VHCs) define the joint angles as functions of a time-invariant quantity called a phase variable [17]. VHCs have been used to replicate human walking gaits [6], [18]–[21] and traverse uneven environments (e.g., stairs [22] and obstacles [5]) using this time-invariant representation of locomotion. Due to their fixed kinematic patterns, an inherent challenge with VHCs is dealing with task changes. We previously showed that holonomic outputs/trajectories need to be updated as speed changes to deliver appropriate ankle and knee work [20]. All holonomic virtual constraints have this fundamental limitation and thus require some sort of finite state machine or higher-dimensional kinematic model (e.g., [23]–[25]) to adjust kinematics based on task. Additionally, by definition VHCs cannot adjust to velocity-dependent variability in gait. However, nonholonomic virtual constraints (NHVCs) have the potential to address some of the fundamental challenges in VHCs.

NHVCs are a variant of virtual constraints that encode velocity-dependent walking gaits via momenta conjugate to the unactuated degrees-of-freedom of the bipedal robot [26]–[30]. NHVCs have been shown to be robust to external perturbations [26], statistically more robust than traditional VHCs [28], and capable of representing distinct walking trajectories for different terrains [30]. NHVCs have also been successfully implemented on the biped MARLO [27]. Motivated by these recent advances, this work seeks to leverage the unique properties of NHVCs to design a single controller capable of representing multiple desired stance-phase trajectories across distinct walking speeds for a powered prosthetic leg.

Contributions of the paper: We extend the application of NHVCs to walking with a powered prosthesis across a range of walking speeds. Specifically, the main contributions are as follows: (1) We present a method for designing stance-phase NHVCs from human subjects data [24] using the dynamic model from [31] to obtain the segmental momentum conjugate to the unactuated degree of freedom (DOF) for the

This work was supported by NSF Awards 1652514 / 1949869 and 1637704 / 1854898 and by the National Institute of Child Health & Human Development of the NIH under Award Number R01HD094772. The content is solely the responsibility of the authors and does not necessarily represent the official views of the NIH or NSF. R. D. Gregg IV, Ph.D., holds a Career Award at the Scientific Interface from the Burroughs Wellcome Fund.

J. C. Horn is with the Department of Mechanical Engineering and Department of Bioengineering, University of Texas at Dallas, Richardson, TX 75080, USA. Contact: jch160630@utdallas.edu

R. D. Gregg is with the Department of Electrical Engineering and Computer Science and the Robotics Institute, University of Michigan, Ann Arbor, MI 48109 USA. Contact: rdgregg@umich.edu

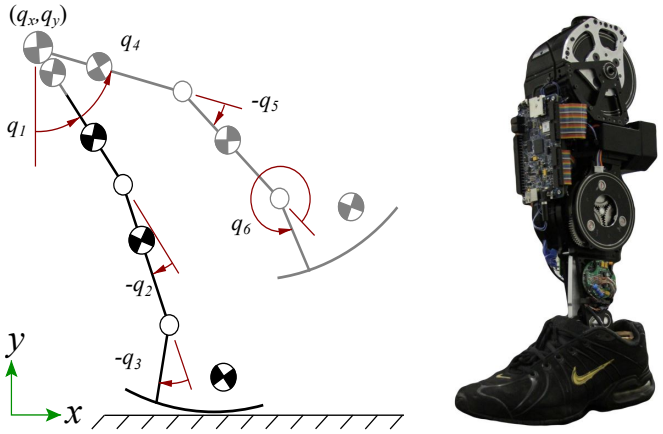

Fig. 1. Left: Configuration space of the human-prosthesis model, reproduced from [31]. The human subsystem is shown in grey, while the prosthetic subsystem is shown in black. Right: Final assembly of the Quasi-Direct Drive Leg, reproduced from [32].

prosthetic subsystem. For the swing phase, we use a VHC due to the limited sensing capabilities of the prosthetic device (the momentum conjugate to the unactuated DOF cannot be calculated during swing). (2) We formulate an optimization problem that fits a single NHVC output to stance-phase human walking data for a finite set of walking speeds. (3) We achieve the first experimental implementation of NHVCs on a powered prosthetic leg, and show that the controller produces natural variability in prosthetic joint angles due to both temporal and kinematic variation of the (able-bodied) human user.

The paper is organized as follows. Sec. II reviews the preliminaries from the NHVC framework and introduces the parameterization for the virtual constraints. Sec. III presents an optimization-based methodology for designing a single NHVC for distinct walking speeds based on experimental human data from [24]. Additionally, Sec. III presents the control scheme that is implemented in a previously-designed powered prosthetic leg. Sec. IV presents an experimental study with an able-bodied human test subject. This study verifies the ability of the NHVC to accurately represent the walking trajectories of three different walking speeds. We investigate the observed findings of trajectory variation over the stance phase of the gait cycle. Finally, Sec. V discusses these results and Sec. VI provides concluding remarks and future research directions.

II. Modeling and Preliminaries

In this section we briefly introduce the dynamics used to model the human-prosthesis system with one degree of underactuation (first proposed and presented in [31]). We also present the class of NHVCs that are used in this work [26], [28]. Lastly, we present the method for parameterizing the virtual constraints for different stages of the gait cycle.

A. Powered Knee-Ankle Prosthesis Model

For this work, we focus on the prosthesis subsystem of the planar human-prosthesis biped in Fig. 1. In the model introduced in [31], each subsystem has its own set of generalized coordinates. The degrees of freedom for the prosthesis subsystem are $q = [q_x, q_y, q_1, q_2, q_3]^T$, where q_1 is the absolute thigh angle, q_2 and q_3 are the relative knee and ankle angles, and (q_x, q_y) is the Cartesian hip position. The dynamics of the prosthesis subsystem can be written as [31]

$$M(q)\ddot{q} + C(q,\dot{q})\dot{q} + G(q) + E(q)^T\lambda = Bu + J(q)^T F, \quad (1)$$

where $M(q) \in \mathbb{R}^{5\times5}$ is the inertia matrix, $C(q,\dot{q}) \in \mathbb{R}^{5\times5}$ is the Coriolis/centrifugal matrix, and $G(q) = \frac{\partial V}{\partial q} \in \mathbb{R}^5$ is the vector of gravitational forces based on the potential energy $V(q)$. The matrix $E(q) \in \mathbb{R}^{2\times5}$ is the Jacobian of two physical constraints modeling rolling foot contact with the ground, which approximates foot compliance [18]. The Lagrange multiplier $\lambda \in \mathbb{R}^2$ represents the associated ground reaction forces (GRF). The matrix $B = [0_{2\times3}, I_{2\times2}] \in \mathbb{R}^{5\times2}$ maps the control torques into the dynamics and has full rank 2. The socket interaction force/moment vector $F = [F_x, F_y, M_z]^T$ is exerted at the mid-thigh connecting the prosthesis and the human [31].

B. Holonomic and Nonholonomic Virtual Constraints

Virtual constraints, presented formally in [17], are kinematic relations between robot joint variables that impose a time-invariant locomotion pattern [33]–[36]. Typically, a VHC of the joint kinematics is defined with a general output function of the following form:

$$y = \xi_0 q - h_{\mathrm{h}}(\theta(q)), \quad (2)$$

where matrix ξ_0 selects the coordinate(s) being controlled, $\theta(q)$ is a monotonic function of the configuration variables that takes values between 0 and 1 along the designed gait, and h_{h} is the functional relationship of the joint variables that describes the desired motion. The goal of the controller is then to drive each joint's output function to zero to achieve the desired time-invariant joint trajectory.

A framework for velocity-dependent, nonholonomic virtual constraints (NHVCs) was recently introduced in [27]–[29], [37] to increase adaptability and robustness. This framework constructs nonholonomic constraints utilizing the momentum conjugate to the unactuated DOF q_{u} (i.e., q_1 in Fig. 1). This conjugate momentum is defined as

$$\sigma_{\mathrm{u}}(q,\dot{q}) = B^{\perp}M(q)\dot{q}, \quad (3)$$

where $B^{\perp} \in \mathbb{R}^{1\times5}$ is the full-rank annihilator matrix for B, such that $BB^{\perp} = 0$. The momentum term σ_{u} is only affected by the conservative forces acting on the biped system as a result of potential energy and not control inputs. If the output depends on velocity only through this term, then variable substitution of the Lagrangian (see [28], [30]) gives rise to a relative degree-two output. In other words, the torque input only appears after taking two derivatives of the output, giving us control over both the joint positions and velocities. This motivates us to express a NHVC as an output function of the configuration vector q and the momentum term σ_u:

$$y = \xi_0 q - h_{\mathrm{nh}}(q, \sigma_{\mathrm{u}}(q,\dot{q})). \quad (4)$$

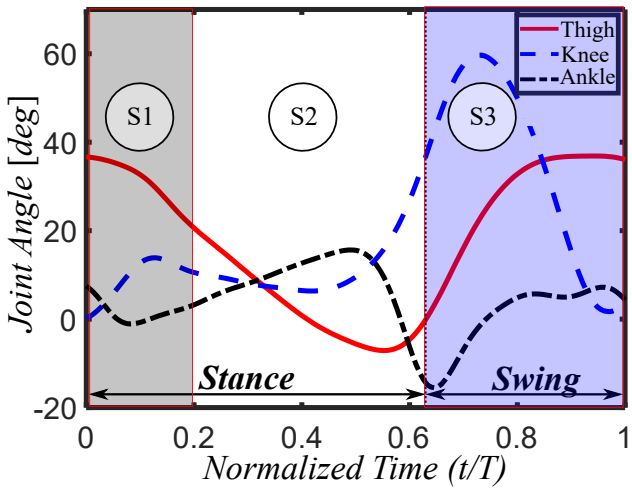

Fig. 2. Human leg joint angles for one stride at 1.0 m/s for an entire walking stride (stance and swing) [24]. S1 corresponds to the touchdown state, S2 corresponds to mid-to-late stance, and S3 corresponds to swing state of the control strategy.

C. Defining the Phase Variable

In this subsection we will introduce the method used to parameterize our outputs. We present three phases of locomotion, and outline the use of two distinct phase variables.

We begin this process by outlining the definition of the phase variable. The function must be: 1) monotonic, 2) smooth and continuous, and 3) measurable from onboard prosthesis sensors [17]. Of these three requirements, the third poses the biggest hurdle in the design of NHVCs. For this work, we will consider the powered knee-ankle prosthesis in Fig. 1 (right), designed by Elery et al. [32]. The knee and ankle actuators of the prosthetic device each have an optical quadrature encoder to measure joint angles/velocities, a 6-axis load cell is located below the ankle joint axis to detect ground contact, and an inertial measurement unit (IMU) above the knee axis measures the orientation of the residual thigh. If we compare the sensing capabilities of the prosthesis to Fig. 1 (left), we can reliably measure q_1, q_2, and q_3, and we can calculate q_x and q_y during the prosthesis stance phase through forward kinematics. During swing phase, we cannot reliably access q_x and q_y due to IMU drift in these coordinates. Therefore, we will choose a phase variable that only utilizes the residual thigh angle and the joint angles of the prosthetic knee and ankle.

Fig. 2 shows the thigh, knee, and ankle angles plotted for an entire stride for an able-bodied subject over flat ground [24]. None of these angles are monotonic throughout the entire stance phase. However, we can utilize distinct phase variables for the stance phase and the swing phase, $\theta(q)$ and $\tau(q)$, respectively. We additionally use a state to ensure a smooth transition from swing to stance phase, denoted as touchdown. We consider this state first.

S1: Touchdown Phase. We first define $\theta(q)$ using the normalized horizontal position of the hips. That is,

$$\theta(q) = \frac{q_x - q_x^+}{q_x^- - q_x^+} \tag{5}$$

where q_x^- is the nominal value of the hip position just before contralateral foot impact (end of prosthetic stance phase), and q_x^+ is the nominal value of the hip position just after prosthetic foot impact (start of prosthetic stance phase). We define these normalization parameters based on the nominal, horizontal range of motion from across-subject average walking data at a speed of 1 m/s [24]. The horizontal hip position is indeed monotonic and can be calculated through forward kinematics with the stance leg joint angles.

The Touchdown Phase is defined as $0 < \theta(q) < 0.2$, which represents the swing to stance transition immediately after the prosthetic foot impacts the ground. While the knee is controlled according to the designed NHVC, we set the ankle set-point to zero to prevent a sudden change in commanded position during the impact event (when momentum changes quickly). The human ankle trajectory approximately aligns with zero at $\theta(q) = 0.2$ for a walking speed of $v = 1.0$ m/s (see Fig. 2), which offers a natural transition point to the Mid-to-Late Stance Phase. Although this alignment may not be perfect across walking speeds, setting the ankle set-point to zero offers an impedance-like controller that will compliantly accommodate temporal variations in the touchdown phase. Additionally, since the knee NHVC is the same for both Touchdown and Mid-to-Late Stance phases, the timing of this transition does not matter for the knee.

S2: Mid-to-Late Stance Phase. This period uses the hip phase variable $\theta(q)$ with the designed NHVC for both the knee and ankle. Mid-to-Late Stance Phase persists until the stance foot leaves the ground.

S3: Swing Phase. We now introduce a phasing variable for use with a VHC during the swing period. Specifically, we will use the same variable presented in [5] that uses the ascending and descending trajectory of the thigh angle to construct a monotonic function. The swing period includes most of the ascending portion and a small part of the descending portion (Fig. 2). Therefore, the swing phase variable is defined by

$$\tau(q) = \begin{cases} \frac{q_1^0 - q_1}{q_1^0 - q_1^{\min}}, & \text{descending} \\ 1 + \frac{1 - s_{\mathrm{m}}}{q_1^0 - q_{1,\mathrm{m}}}(q_1 - q_1^0), & \text{ascending} \end{cases} \tag{6}$$

Here, q_1^0 and $q_1^{\min}$ are constants of the thigh angle at touchdown and the minimum thigh value, respectively. The dynamic reset variables s_{m} and $q_{1,\mathrm{m}}$ represent the values of the phase variable and thigh angle at the point of transition from descending to ascending, respectively. A dynamic reset variable changes value based on the previous step and continues to update after each step. The intent of a dynamic reset variable is to account for stride-to-stride variance in human locomotion, and in our case ensures smooth transitions between ascending and descending phases of the thigh angle.

D. Segmental Conjugate Momentum

The conjugate momentum can be expressed as [17]

$$\sigma_{\mathrm{u}}(q, \dot{q}) = B^{\perp} M(q) \dot{q} = \frac{1}{2} \dot{q}^T \frac{\partial M}{\partial q_u} \dot{q} - \frac{\partial V}{\partial q_u}. \tag{7}$$

Since we do not have information from the healthy human limbs (i.e., q_4, q_5, and q_6 in Fig. 1), we use the segmental momentum (i.e., the conjugate momentum for individual segments rather than the entire system) conjugate to the

unactuated degree of freedom. For the prosthesis system, we calculate σ_{u} using the potential energies of the prosthetic pylon connected to the residual thigh, prosthetic shank, and prosthetic foot. That is,

$$\sigma_{\mathrm{u}}(q,\dot{q}) = \sigma_{\mathrm{u,foot}} + \sigma_{\mathrm{u,shank}} + \sigma_{\mathrm{u,thigh}}. \tag{8}$$

This term is not normalized like the phase variable because it is not monotonic and does not represent stride progression. We model the segmental conjugate momentum using the prosthesis parameters from [32].

III. Control Design

This section presents the methodology for the design of NHVCs that will enable locomotion across walking speeds. We set up the NHVC design procedure via an optimization problem that fits healthy human walking trajectories from a publicly available dataset [24]. We then formulate an optimization problem for designing a VHC during the swing phase of locomotion.

A. Stance Phase NHVCs

Consider a finite set of possible walking speeds denoted as $\mathcal{V} = \{v_i\}_{i=1}^{m}$, $m \geq 1$. Suppose further that we have desired knee and ankle trajectories for human walking at each $v_i \in \mathcal{V}$. Our objective is to design a single nonholonomic output for each joint that represents the stance portion of these trajectories across $\mathcal{V}$. For this purpose, we consider a vector output y_{nh} of the form (4) with $\xi_0 := [0_{2\times 3}, I_{2\times 2}]$, and define $h_{\mathrm{nh}}(\theta,\sigma_{\mathrm{u}}) = [h_{\mathrm{nh,ankle}}(\theta,\sigma_{\mathrm{u}}), h_{\mathrm{nh,knee}}(\theta,\sigma_{\mathrm{u}})]^T$ as

$$h_{\mathrm{nh}}(q,\sigma_u) := \sum_{i=0}^{k} b_i\theta^i(q) + \sum_{i=0}^{k} \kappa_i\theta^i(q)\sigma_{\mathrm{u}}, \tag{9}$$

where $\kappa := [\kappa_0\, \kappa_1\, \cdots\, \kappa_k]$ represents the coefficient matrix of the nonholonomic terms of the polynomial, and $b := [b_0\, b_1\, \cdots\, b_k]$ represents the coefficient matrix of the holonomic terms. This choice of polynomial is motivated by the sensing capabilities of the prosthesis. In order to calculate the joint velocities in σ_{u}, the leg's microcontroller computes a numerical derivative for each angle signal. This technique is susceptible to amplifying noise [38], which would get amplified by higher powers of σ_{u}. Therefore, we chose not to use higher powers of σ_{u} in the polynomial. Additionally, we choose $k = 5$ in (9) for an adequate trade-off between fitting accuracy and computational complexity in the implementation.

In our case study, we optimize κ and b to design NHVCs that represent the joint trajectories for three different walking speeds: $\mathcal{V} = \{0.8, 1.0, 1.2\}$ m/s. The walking trajectories were obtained from the across-subject averages of the 10 subjects reported in the data set of [24]. In the following, we use the notation $\hat{(\cdot)}$ to designate a measured data sequence. We take the measured data for the stance periods of all three walking trajectories and form a sequence of data, $\hat{q}_{\mathrm{tot}} = [\xi_0\hat{q}_{v=0.8\mathrm{m/s}}, \xi_0\hat{q}_{v=1.0\mathrm{m/s}}, \xi_0\hat{q}_{v=1.2\mathrm{m/s}}]$, with $\xi_0 = [0_{2\times 3}, I_{2\times 2}]$. We index each data point of $\hat{q}_{\mathrm{tot}}$ with $j = 1,\ldots,s$ where s marks the final entry of the appended data. We then calculate $\theta_{\mathrm{tot},j} = \theta(\hat{q}_{\mathrm{tot},j})$ and $\sigma_{\mathrm{tot},j} = \sigma_{\mathrm{u}}(\hat{q}_{\mathrm{tot},j}, \dot{\hat{q}}_{\mathrm{tot},j})$ over all samples for the following optimization.

Optimization Problem (NHVC): Find b and κ to minimize the sum of distances between the measured ankle and knee data points, $\hat{q}_{\mathrm{tot},j}$, and the corresponding points of the parameterized surface, $h_{\mathrm{nh}}(\theta_{\mathrm{tot},j}, \sigma_{\mathrm{tot},j})$. Specifically, the problem is

$$\arg\min_{b,\kappa} \sum_{j=1}^{s} ||\hat{q}_{\mathrm{tot},j} - h_{\mathrm{nh}}(\theta_{\mathrm{tot},j}, \sigma_{\mathrm{tot},j})||_2^2, \tag{10}$$

subject to the joint range-of-motion constraints

$$[-35^\circ; -1^\circ] \leq h_{\mathrm{nh}}(\theta_{\mathrm{tot},j}, \sigma_{\mathrm{tot},j}) \leq [20^\circ; 70^\circ], \forall\ j. \tag{11}$$

B. Swing Phase VHC

As previously noted, the NHVCs in this work are only implementable during the prosthesis stance phase, so we instead design a VHC to control the prosthesis during its swing phase. For this purpose, we consider a VHC vector output

$$y_{\mathrm{h}} = \xi_0 q - h_{\mathrm{h}}(\tau(q)), \tag{12}$$

where $h_{\mathrm{h}}(\tau) = [h_{\mathrm{h,ankle}}(\tau), h_{\mathrm{h,knee}}(\tau)]^T$ is defined by

$$h_{\mathrm{h}}(\tau(q)) := \sum_{n=0}^{M} \alpha_n \frac{M!}{n!(M-n)!}\tau^n(1-\tau)^{M-n}. \tag{13}$$

Here, α_n represents the coefficient matrix of the Bézier polynomial. The order of the polynomial is chosen as $M = 6$. The VHC is designed from the across-subject average trajectory for the swing period of walking at $v_i = 1.0$ m/s, which we designate as the sequence $\hat{q}_{\mathrm{sw}}$. We index this sequence by j for $j = 1,\ldots,z$, with z indicating the end of the sequence. We then calculate $\tau_{\mathrm{sw},j} = \tau(\hat{q}_{\mathrm{sw},j})$ over these samples for the following optimization.

Optimization Problem (VHC): Find an optimal α to minimize the sum of distances between the measured ankle and knee data points, $\hat{q}_{\mathrm{sw}}$, and the designed holonomic parameterization, $h_{\mathrm{h}}(\tau_{\mathrm{sw},j})$. Specifically, our problem is stated as

$$\arg\min_{\alpha} \sum_{j=1}^{z} ||\hat{q}_{\mathrm{sw},j} - h_{\mathrm{h}}(\tau_{\mathrm{sw},j})||_2^2 \tag{14}$$

subject to the constraint $h_{\mathrm{h}}(\tau_{\mathrm{sw},1}) = h_{\mathrm{nh}}(\theta_{\mathrm{tot},\rho}, \sigma_{\mathrm{tot},\rho})$ where ρ is the final sample of the stance period for $v_i = 1.0$ m/s. I.e., the initial value of the holonomic parameterization is equal to the final value of the nonholonomic parameterization for $v_i = 1.0$ m/s. Additionally, the joint angles are constrained by

$$[-35^\circ; -1^\circ] \leq h_{\mathrm{h}}(\tau_{\mathrm{sw},j}) \leq [20^\circ; 70^\circ], \forall\ j. \tag{15}$$

C. Data Driven Output Design

The `fmincon` function in MATLAB is used to compute the coefficients b, κ, and α for the stance and swing phase outputs. The time to solve both the NHVC and VHC optimization problems is approximately 0.5-1 minutes, using an Intel Core i7-4770 processor. For this work, the result of the nonholonomic optimization will be noted as NHVC-HI (human inspired). The resulting kinematic surface h_{nh} is shown in Fig. 3, where the prescribed knee and ankle angles are plotted against the phase variable $\theta(q)$ and momentum $\sigma_u(q,\dot{q})$. The coefficient of determination for each output (compared to the average trajectories) is 0.9765 for the ankle, and 0.9804 for the knee.

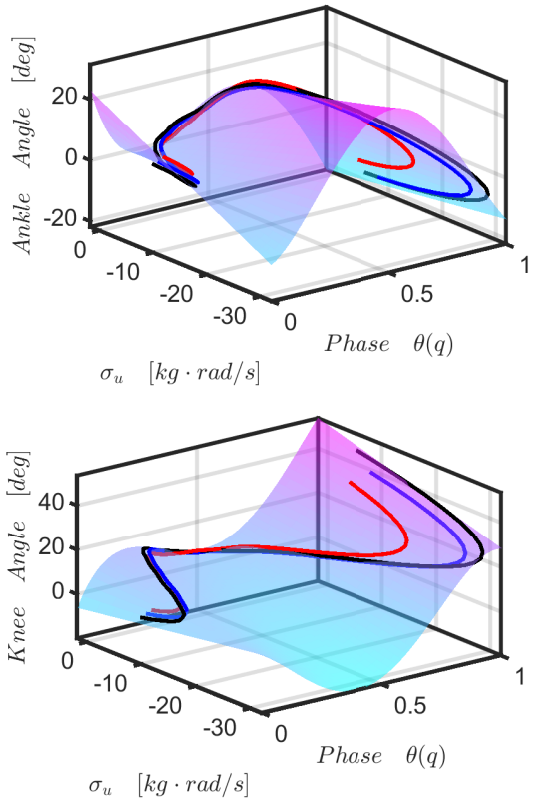

Fig. 3. Average ankle (top) and knee (bottom) trajectories for all human subjects for 0.8 (black), 1.0 (blue), and 1.2 m/s (red) plotted against the designed NHVC surface.

D. Control Scheme

With the definition of the phase variables and virtual constraints now in hand, the next step is to define the control law. The desired knee and ankle angles are taken from the previously defined virtual constraints and will be imposed using a Proportional-Derivative (PD) controller. The expression for commanded motor torque is given by

$$u = k_{\mathrm{p},r} y_r + k_{\mathrm{d},r} \dot{y}_r, \tag{16}$$

where $k_{\mathrm{p},r} > 0$ is the proportional gain for joint r applied to the joint tracking error y_r, and $k_{\mathrm{d},r} > 0$ is the derivative gain corresponding to joint r that is applied to the time derivative of the tracking error, $\dot{y}_r$. These gains will be tuned in Section IV-A. The tuned gains are used for both stance and swing phases during the experiment, and the values are never changed after the tuning procedure.

IV. Experimental Results

In this section, we experimentally verify the performance of our proposed control scheme. We will present experimental results for two scenarios: 1) steady-state locomotion at three distinct walking speeds, and 2) walking speed variation across the same three speeds. A supplemental video of the experiments is available for download [39].

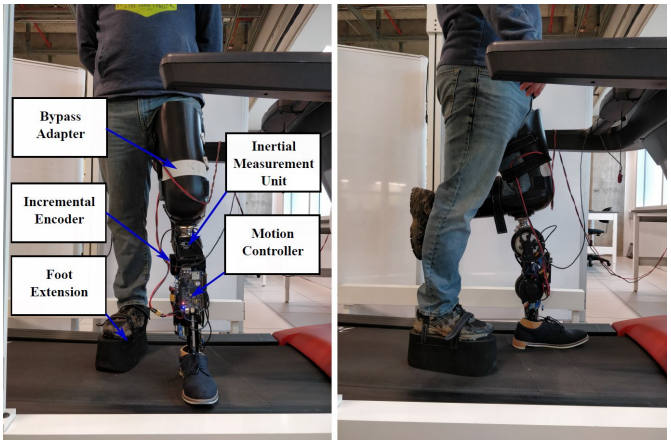

Fig. 4. Component diagram of the human subject and powered prosthesis experimental setup.

A. Experimental Setup

The prosthetic device uses a 22:1 custom made SPC-PGT transmission paired with a frameless, brushless ILM 85×26 DC motor kit. The device is capable of supplying 57.2 Nm of continuous torque and 182.6 Nm of peak torque using this configuration. The device utilizes E5 and EC35 optical incremental encoders for each motor. Elmo Motion controllers are used to drive the motors and read the encoder values. Additionally, a M3564F 6-axis load cell located at the base of the foot measures the reaction forces that are used to determine ground contact. The controller is implemented on an onboard National Instruments myRIO microcontroller. The prosthetic device is powered by four TP1600-4SA80X LiPo batteries. With all sensors and batteries included, the prosthetic device has a final mass of 6.09 kg.

The controller was tested through a set of walking experiments over level ground with an able-bodied human subject. The participant donned the prosthesis by wearing a bypass adapter over their knee (Fig. 4). The test subject was a 29 year old male with a height of 1.78 m and a mass of 81.65 kg. The participant had no prior experience with the control scheme being tested on the prosthesis. The experimental protocol was reviewed and approved by the Institutional Review Board (IRB) at the University of Texas at Dallas (protocol 17-128, approved on July 19, 2019).

All experiments were performed on a powered treadmill with a safety harness. The control gains in Sec. III were adjusted to achieve desired performance (sufficient push-off, trajectory tracking, and comfort) during acclimation trials before data collection, and then remained fixed. The subject was given time to rest as needed between the walking trials described below. Fig. 4 shows the technical diagram and the experimental setup used during data collection.

B. Steady State Locomotion

The purpose of this experiment was to verify that the NHVC-HI produces walking trajectories that correspond to the reference data. The human subject walked on a level treadmill at three distinct speeds that match the design speeds: slow (0.8

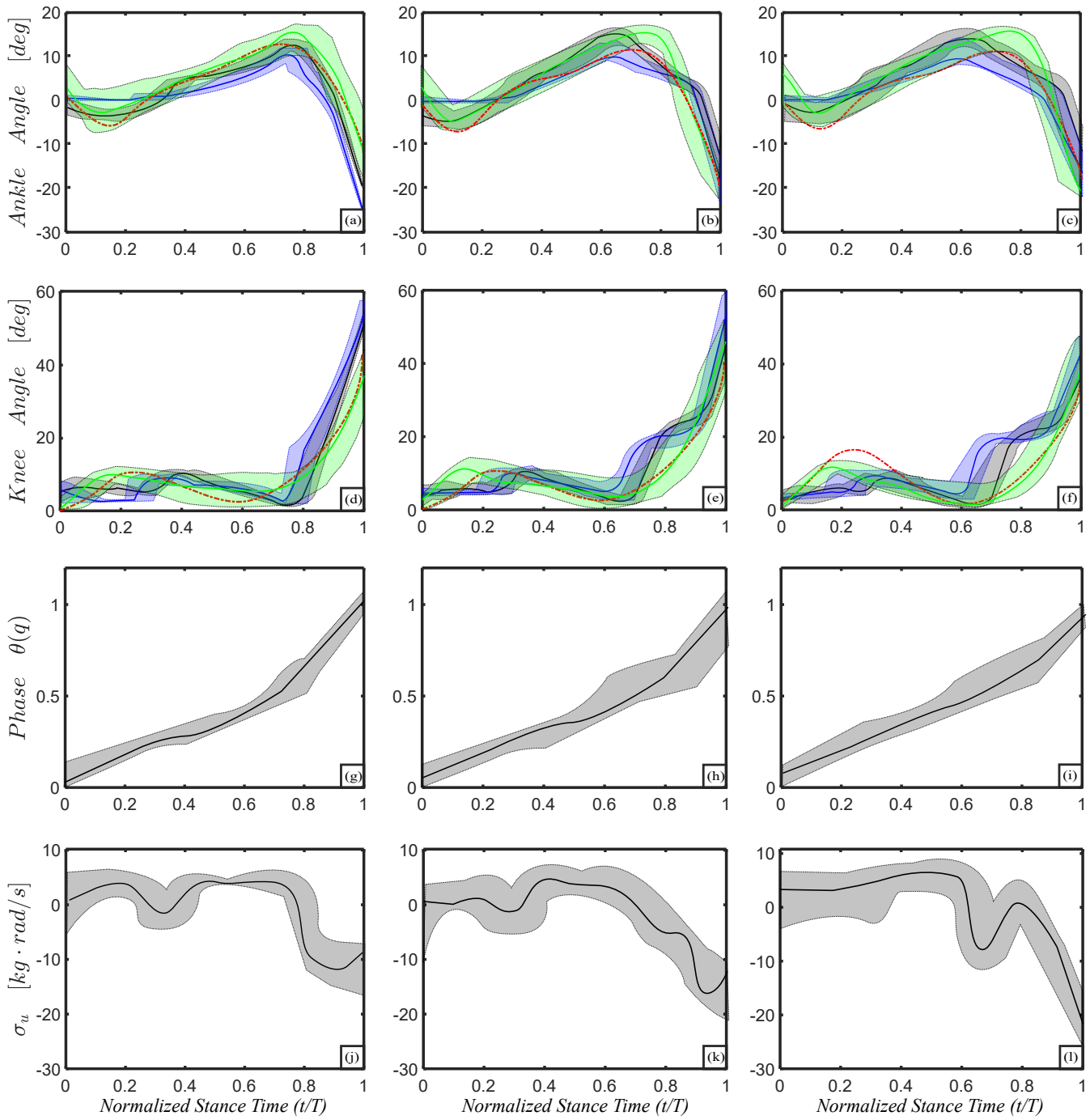

Fig. 5. Experimental results during the stance phase for steady-state walking at $v_i = 0.8$ m/s (left), $v_i = 1.0$ m/s (center), and $v_i = 1.2$ m/s (right). Blue corresponds to commanded joint angle, black (and gray shaded region) corresponds to measured signal, green corresponds to normative data for able-bodied subject AB05 in [24], and red is the reference human trajectory (i.e., average trajectory across human subjects at the corresponding speed). The solid color lines represent the average over the walking trial, and the shaded region reflects the maximum and minimum values. Each speed condition had $n_{0.8\mathrm{m/s}} = 17$, $n_{1.0\mathrm{m/s}} = 22$, and $n_{1.2\mathrm{m/s}} = 28$ steps.

m/s), normal (1.0 m/s), and fast (1.2 m/s). Data was logged for 30 seconds at each speed, and data collection started once the participant produced a reasonably consistent gait cycle rhythm (i.e., *steady-state* locomotion).

Fig. 5 shows the results from these trials, focusing on the stance period when the NHVC was used. For all walking speeds, the commanded trajectory indeed varies between strides based on the momentum throughout the stance phase of the gait cycle. Additionally, the range of maximum/minimum commanded trajectory values gradually increase as the walking speed increases. The onset of plantar flexion (and the peak ankle angle) occurs earlier in the stance phase as the speed increases, which is a normative trend in human locomotion [5], [40]. This behavior is associated with a decrease in the stance to swing ratio (approaching even) [41].

Fig. 6 shows the range of commanded ankle angles against

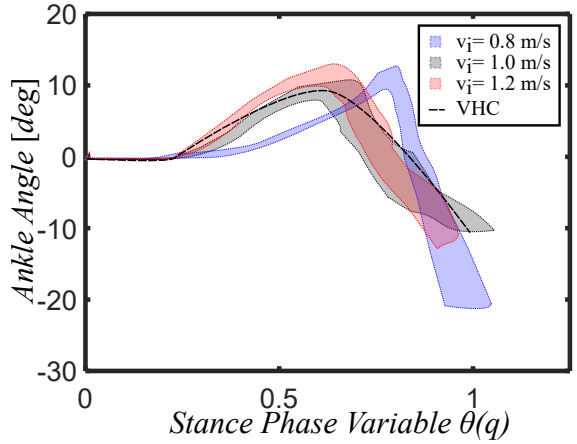

Fig. 6. Range of commanded ankle angles for each walking speed over the stance phase variable. The dashed line represents an example VHC.

the phase variable $\theta(q)$ for all speeds. We note that for each speed, we see variance in the commanded joint angle over the stance phase. This contrasts with the case of a VHC controller, where the virtual constraint is uniquely defined for any given phase variable value by definition (i.e., the commanded trajectory will have no variance with respect to phase) as seen by the dashed line in Fig. 6. When the trajectory commanded by a VHC is plotted over normalized time, the variance can be attributed to the pace at which the subject progresses through the gait cycle (as seen in [5]). Fig. 6 shows that the variance in NHVC joint angle in Fig. 5 is not only a product of temporal variation, but also a product of kinematic changes by the subject. These kinematic changes are captured in the momentum term shown the last row of Fig. 5. Note that the commanded joint angles in Fig. 6 correspond to the designed NHVC surfaces depicted in Fig. 3.

C. Walking Speed Variation

We also performed a stepped velocity transition experiment to show that the NHVC is capable of adapting the walking trajectories in real time. This experiment involved treadmill walking in a continuous sequence of the following speeds (10 seconds each): 0.8 m/s, 1.0 m/s, 1.2 m/s, 1.0 m/s, and 0.8 m/s. This resulted in 50 seconds of data collection with $n_{0.8\mathrm{m/s}} = 9$, $n_{1.0\mathrm{m/s}} = 15$, and $n_{1.2\mathrm{m/s}} = 10$ steps for each speed.

Fig. 7 shows all strides of the stepped speed variation experiment. The stance phase data shows the NHVC-HI controller indeed produces appropriate walking trajectories with similar variation to the reference able-bodied subject data from [24]. In contrast, the swing phase VHC does not produce similar variation to the reference subject. Finally, Fig. 7 shows that the NHVC exhibits a similar shift in the onset of plantar flexion as seen in the steady state experiment. This is observable through the peak ankle angle during the stride, and the three distinct peak clusters of the trajectories.

Fig. 8 shows the joint work per stride across all speeds. The knee joint performed negative work and progressively increased in magnitude with speed. The ankle joint performed positive work and similarly increased in magnitude with speed. Both of these are normative trends [42], [43]; the ankle

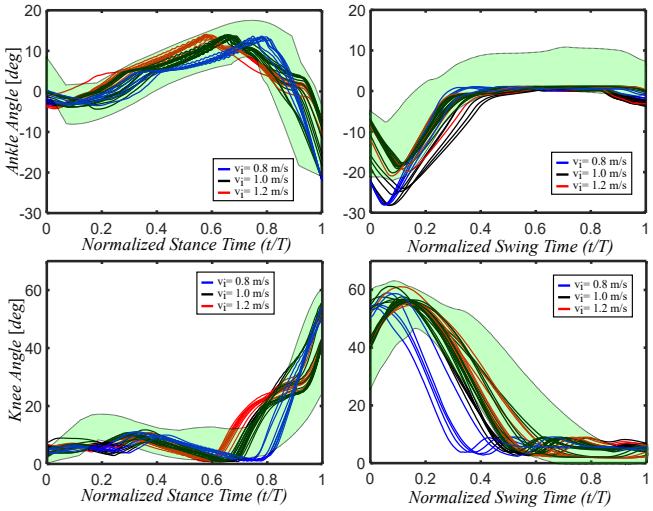

Fig. 7. Stepped walking speed variation results for the total gait cycle. Measured ankle (Top) and knee (bottom) joint angles for all strides of the human subject. The shaded region corresponds to the combined maximum and minimum values for reference subject AB05 from [24] across all three speeds. Stride trajectories are colored based on the speed of the treadmill.

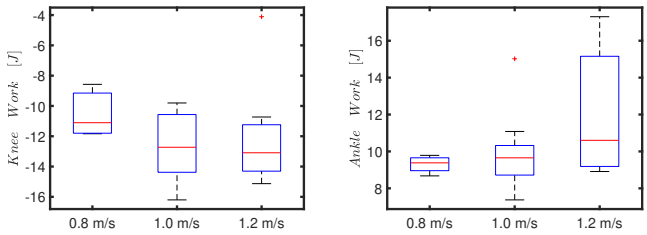

Fig. 8. Box plots of stance-phase work of the prosthetic knee (left) and ankle (right) during stepped walking speed experiment.

and knee are providing the necessary adjustments in energy injection and absorption, respectively, to adapt to changes in walking speed. This is reflected by the average observed torques for each walking speed in Fig. 9. We also note that variance in joint work tends to increase with walking speed, which reflects the higher physical demand to maintain both propulsion and stability.

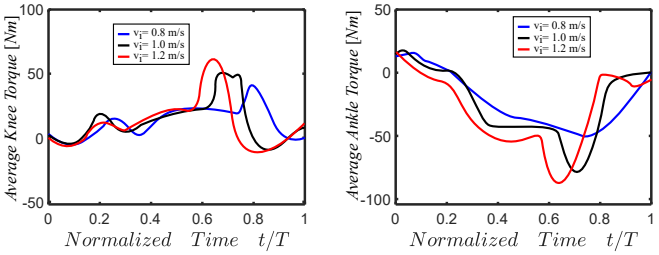

Fig. 9. Average knee (left) and ankle (right) torque of the prosthesis during stepped walking speed experiment.

V. Discussion

The goal of this study was to design a single NHVC controller to accurately represent the stance phase joint trajectories of three different walking speeds, without the need for switching logic or reset variables. We hypothesized that

parameterizing the virtual constraints with two variables—θ depending on joint positions and σ_{u} also depending on joint velocities—would enable accurate representation of the desired trajectories.

A. Advantages of NHVCs

The main benefit of NHVCs is the ability to encapsulate a set of desired trajectories with one functional expression. Existing control approaches for powered prostheses require switching logic between different controllers [18]–[20] or interpolation between reference trajectories [8], [25] to naturally adapt kinematics to different walking speeds. The use of NHVCs removes these complexities, and relies on the proper design of one single output.

The results indicate that the NHVCs reproduce normative joint trajectories with stride-to-stride varinace based on the temporal as well as kinematic (conjugate momentum) changes. Although the optimization problem considered kinematic variance over three walking speeds, it did not directly consider stride-to-stride variance at any given speed. The NHVCs produce stride-to-stride variance as a consequence of the two-dimensional parameterization, i.e., small changes in momentum cause corresponding changes in joint kinematics. This could potentially be used to accommodate more trajectories than the controller was originally designed for, including human kinematic variability and untrained speeds. Future studies will investigate whether the proposed NHVCs can appropriately respond to the increased variability and loss of local stability and predictability in the walking gait patterns of lower-limb amputee users [44].

In addition to kinematic adaptations, the NHVCs produced appropriate kinetic adaptations to changes in walking speed (Fig. 8). Our prior work [20] found that VHCs enable user synchronization during speed changes (by virtue of the phase variable), but joint work does not adapt appropriately with fixed VHC output functions. NHVCs overcome this limitation by modulating joint kinematics as a function of the conjugate momentum, which changes with walking speed. These kinematic adaptations, combined with user synchronization through the phase variable, enable appropriate kinetic adaptations with fixed NHVC outputs. However, future studies with amputee participants are needed to verify these benefits extend to the intended use case.

B. Limitations of NHVCs

The primary limitation of NHVCs is their susceptibility to noise in the velocity measurements. Numerical derivatives magnify the noise in the joint encoder measurements, and IMU measurements of angular velocity are inherently noisy. We dealt with this challenge by restricting the NHVC to a low-order parameterization (excluding powers of $\sigma_{\mathrm{u}} = B^{\perp}M(q)\dot{q}$ greater than one). Future work could investigate the use of advanced filtering and observer techniques such as [45], [46] to reduce noise and enable the use of higher-order NHVC parameterizations.

Second, the NHVC surfaces in Fig. 3 are designed for a specific range of values for σ_{u}, outside of which the predicted joint angles could become erratic. This is also a problem with respect to the phase variable of both VHCs and NHVCs. Phase variables are often saturated outside of their design range [5], [17], and this could also be done with the conjugate momentum. Additionally, increasing the set of reference trajectories in the design optimization will result in NHVC surfaces that represent a larger range of possible walking trajectories. However, the presented optimization method only considers across-subject average trajectories (e.g., from the data presented in [24]) which does not yield optimal user-specific performance. This approach can potentially be improved through the use of subject-specific tuning (e.g., [47]) or with the application of model predictive control [48].

Third, the presented NHVC control scheme is only applicable to the stance phase of the walking gait. Measuring the conjugate momentum during swing would require measurements of the sound leg, but it is generally thought that powered prosthetic legs must be self-contained to be clinically viable [18], [20], [49]. One method to extend NHVCs to the swing phase while using only onboard sensors is through model-based, observers [50]–[52], which is left to future work.

VI. Conclusion and Future Research

The primary goal of this work was to design a NHVC controller capable of producing distinct walking trajectories for different walking speeds. Using the unactuated conjugate momentum for the prosthesis, an optimization problem was used to design a single NHVC for three distinct walking speeds. Physical experiments for steady-state walking and stepped velocity transitions show that the NHVC control scheme was capable of accurately representing reference trajectories used in the design phase. The control scheme produced appropriate joint variability due to stride-to-stride variability of the human user, despite not being explicitly considered in the design phase. In future work we plan to extend this approach to multiple terrain environments and validate these control strategies with amputee participants.

References

[1] M. Rabuffetti, M. Recalcati, and M. Ferrarin, "Trans-femoral amputee gait: Socket–pelvis constraints and compensation strategies," *Prosthetics and orthotics international*, vol. 29, no. 2, pp. 183–192, 2005.

[2] K. Ziegler-Graham, E. J. MacKenzie, P. L. Ephraim, T. G. Travison, and R. Brookmeyer, "Estimating the prevalence of limb loss in the united states: 2005 to 2050," *Archives of physical medicine and rehabilitation*, vol. 89, no. 3, pp. 422–429, 2008.

[3] R. R. Torrealba and E. D. Fonseca-Rojas, "Toward the development of knee prostheses: Review of current active devices," *Applied Mechanics Reviews*, vol. 71, no. 3, 2019.

[4] C. Jayaraman, S. Hoppe-Ludwig, S. Deems-Dluhy, M. McGuire, C. Mummidisetty, R. Siegal, A. Naef, B. E. Lawson, M. Goldfarb, K. E. Gordon *et al.*, "Impact of powered knee-ankle prosthesis on low back muscle mechanics in transfemoral amputees: A case series," *Frontiers in Neuroscience*, vol. 12, p. 134, 2018.

[5] S. Rezazadeh, D. Quintero, N. Divekar, E. Reznick, L. Gray, and R. D. Gregg, "A phase variable approach for improved rhythmic and non-rhythmic control of a powered knee-ankle prosthesis," *IEEE Access*, vol. 7, pp. 109 840–109 855, 2019.

[6] T. Elery, S. Rezazadeh, E. Reznick, L. Gray, and R. D. Gregg, "Effects of a powered knee-ankle prosthesis on amputee hip compensations: A case series," *IEEE Trans. Neural Systems and Rehabilitation Engineering*, vol. 28, no. 12, pp. 2944–2954, 2020.

[7] F. Sup, A. Bohara, and M. Goldfarb, "Design and Control of a Powered Transfemoral Prosthesis." *The International J. robotics research*, vol. 27, no. 2, pp. 263–273, Feb. 2008.

[8] B. E. Lawson, J. Mitchell, D. Truex, A. Shultz, E. Ledoux, and M. Goldfarb, "A robotic leg prosthesis: Design, control, and implementation," *IEEE Robotics & Automation Magazine*, vol. 21, no. 4, pp. 70–81, 2014.

[9] M. Liu, F. Zhang, P. Datseris, and H. H. Huang, "Improving finite state impedance control of active-transfemoral prosthesis using dempster-shafer based state transition rules," *J. Intelligent & Robotic Systems*, vol. 76, no. 3-4, pp. 461–474, 2014.

[10] A. Mohammadi and R. D. Gregg, "Variable impedance control of powered knee prostheses using human-inspired algebraic curves," *J. computational and nonlinear dynamics*, vol. 14, no. 10, 2019.

[11] F. Zhang, M. Liu, and H. Huang, "Investigation of timing to switch control mode in powered knee prostheses during task transitions," *PLOS one*, vol. 10, no. 7, p. e0133965, 2015.

[12] N. Aghasadeghi, H. Zhao, L. J. Hargrove, A. D. Ames, E. J. Perreault, and T. Bretl, "Learning impedance controller parameters for lower-limb prostheses," in *IEEE Int. Conf. Intelligent Robots Systems*, 2013.

[13] A. M. Simon, K. A. Ingraham, N. P. Fey, S. B. Finucane, R. D. Lipschutz, A. J. Young, and L. J. Hargrove, "Configuring a powered knee and ankle prosthesis for transfemoral amputees within five specific ambulation modes," *PloS one*, vol. 9, no. 6, p. e99387, 2014.

[14] M. R. Tucker, J. Olivier, A. Pagel, H. Bleuler, M. Bouri, O. Lambercy, J. del R Millán, R. Riener, H. Vallery, and R. Gassert, "Control strategies for active lower extremity prosthetics and orthotics: a review," *J. neuroengineering and rehabilitation*, vol. 12, no. 1, p. 1, 2015.

[15] H. Huang, D. L. Crouch, M. Liu, G. S. Sawicki, and D. Wang, "A cyber expert system for auto-tuning powered prosthesis impedance control parameters," *Annals of biomedical engineering*, vol. 44, no. 5, pp. 1613–1624, 2016.

[16] Y. Wen, M. Liu, J. Si, and H. H. Huang, "Adaptive control of powered transfemoral prostheses based on adaptive dynamic programming," in *IEEE Int. Conf. Eng. Med. Biology Society*, 2016, pp. 5071–5074.

[17] E. R. Westervelt, J. W. Grizzle, C. Chevallereau, J. H. Choi, and B. Morris, *Feedback Control of Dynamic Bipedal Robot Locomotion*. Boca Raton: CRC Press, Jun. 2007.

[18] R. D. Gregg, T. Lenzi, L. J. Hargrove, and J. W. Sensinger, "Virtual constraint control of a powered prosthetic leg: From simulation to experiments with transfemoral amputees," *IEEE Trans. Robotics*, vol. 30, no. 6, pp. 1455–1471, 2014.

[19] H. Zhao, J. Horn, J. Reher, V. Paredes, and A. D. Ames, "Multicontact locomotion on transfemoral prostheses via hybrid system models and optimization-based control," *IEEE Trans. Automation Science and Engineering*, vol. 13, no. 2, pp. 502–513, 2016.

[20] D. Quintero, D. J. Villarreal, D. J. Lambert, S. Kapp, and R. D. Gregg, "Continuous-phase control of a powered knee–ankle prosthesis: Amputee experiments across speeds and inclines," *IEEE Trans. Robotics*, vol. 34, no. 3, pp. 686–701, 2018.

[21] O. Harib, A. Hereid, A. Agrawal, T. Gurriet, S. Finet, G. Boeris, A. Duburcq, M. E. Mungai, M. Masselin, A. D. Ames *et al.*, "Feedback control of an exoskeleton for paraplegics: Toward robustly stable, hands-free dynamic walking," *IEEE Control Systems Magazine*, vol. 38, no. 6, pp. 61–87, 2018.

[22] H. Zhao, J. Reher, J. Horn, V. Paredes, and A. D. Ames, "Realization of stair ascent and motion transitions on prostheses utilizing optimization-based control and intent recognition," in *IEEE Int. Conf. Rehabilitation Robotics*. IEEE, 2015, pp. 265–270.

[23] X. Da and J. Grizzle, "Combining trajectory optimization, supervised machine learning, and model structure for mitigating the curse of dimensionality in the control of bipedal robots," *The International J. Robotics Research*, vol. 38, no. 9, pp. 1063–1097, 2019.

[24] K. R. Embry, D. J. Villarreal, R. L. Macaluso, and R. D. Gregg, "Modeling the kinematics of human locomotion over continuously varying speeds and inclines," *IEEE Trans. Neural Systems and Rehabilitation Engineering*, vol. 26, no. 12, pp. 2342–2350, 2018.

[25] K. R. Embry and R. D. Gregg, "Analysis of continuously varying kinematics for prosthetic leg control applications," *IEEE Trans. Neural Systems and Rehabilitation Engineering*, vol. 29, pp. 262–272, 2020.

[26] B. Griffin and J. Grizzle, "Nonholonomic virtual constraints for dynamic walking," in *Decision and Control (CDC), 2015 IEEE 54th Annual Conference on*. IEEE, 2015, pp. 4053–4060.

[27] ——, "Nonholonomic virtual constraints and gait optimization for robust walking control," *The International J. Robotics Research*, vol. 36, no. 8, pp. 895–922, 2017.

[28] J. C. Horn, A. Mohammadi, K. Akbari Hamed, and R. D. Gregg, "Hybrid zero dynamics of bipedal robots under nonholonomic virtual constraints," *IEEE Control Systems Letters*, vol. 3, no. 2, pp. 386–391, 2019.

[29] K. Akbari Hamed and A. D. Ames, "Nonholonomic hybrid zero dynamics for the stabilization of periodic orbits: Application to underactuated robotic walking," *IEEE Trans. Control Systems Technology*, pp. 1–8, 2019.

[30] J. C. Horn, A. Mohammadi, K. A. Hamed, and R. D. Gregg, "Nonholonomic virtual constraint design for variable-incline bipedal robotic walking," *IEEE Robotics and Automation Letters*, vol. 5, no. 2, pp. 3691–3698, 2020.

[31] A. E. Martin and R. D. Gregg, "Stable, robust hybrid zero dynamics control of powered lower-limb prostheses," *IEEE Trans. Automatic Control*, vol. 62, no. 8, pp. 3930–3942, 2017.

[32] T. Elery, S. Rezazadeh, C. Nesler, and R. D. Gregg, "Design and validation of a powered knee–ankle prosthesis with high-torque, low-impedance actuators," *IEEE Trans. Robotics*, 2020.

[33] E. R. Westervelt, J. W. Grizzle, and D. E. Koditschek, "Hybrid zero dynamics of planar biped walkers," *IEEE TAC*, vol. 48, no. 1, pp. 42–56, Jan. 2003.

[34] K. Akbari Hamed and R. D. Gregg, "Decentralized feedback controllers for robust stabilization of periodic orbits of hybrid systems: Application to bipedal walking," *IEEE Trans. Control Systems Technology*, vol. 25, no. 4, pp. 1153–1167, 2017.

[35] A. Mohammadi, E. Rezapour, M. Maggiore, and K. Y. Pettersen, "Maneuvering control of planar snake robots using virtual holonomic constraints," *IEEE Trans. Control Systems Technology*, vol. 24, no. 3, pp. 884–899, 2015.

[36] M. Ahmed, A. Hably, and S. Bacha, "Kite generator system periodic motion planning via virtual constraints," in *IECON 2013-39th Annual Conference of the IEEE Industrial Electronics Society*. IEEE, 2013, pp. 1694–1699.

[37] B. Griffin and J. Grizzle, "Walking gait optimization for accommodation of unknown terrain height variations," in *2015 American control conference (ACC)*. IEEE, 2015, pp. 4810–4817.

[38] M. Mboup, C. Join, and M. Fliess, "Numerical differentiation with annihilators in noisy environment," *Numerical algorithms*, vol. 50, no. 4, pp. 439–467, 2009.

[39] "Nonholonomic virtual constraints for control of powered prostheses across walking speeds," YouTube, 2020, https://youtu.be/ef57lMNT1q8.

[40] S. W. Lipfert, M. Günther, D. Renjewski, and A. Seyfarth, "Impulsive ankle push-off powers leg swing in human walking," *J. experimental biology*, vol. 217, no. 8, pp. 1218–1228, 2014.

[41] D. Quintero, D. J. Lambert, D. J. Villarreal, and R. D. Gregg, "Real-time continuous gait phase and speed estimation from a single sensor," in *2017 IEEE Conference on Control Technology and Applications (CCTA)*. IEEE, 2017, pp. 847–852.

[42] P. DeVita, J. Helseth, and T. Hortobagyi, "Muscles do more positive than negative work in human locomotion," *J. Experimental Biology*, vol. 210, no. 19, pp. 3361–3373, 2007.

[43] M. J. Grey, J. B. Nielsen, N. Mazzaro, and T. Sinkjær, "Positive force feedback in human walking," *The J. physiology*, vol. 581, no. 1, pp. 99–105, 2007.

[44] C. J. Lamoth, E. Ainsworth, W. Polomski, and H. Houdijk, "Variability and stability analysis of walking of transfemoral amputees," *Medical engineering & physics*, vol. 32, no. 9, pp. 1009–1014, 2010.

[45] T. Glad and L. Ljung, "Velocity estimation from irregular, noisy position measurements," *IFAC Proceedings Volumes*, vol. 17, no. 2, pp. 1069–1073, 1984.

[46] T. D. Larsen, K. L. Hansen, N. A. Andersen, and O. Ravn, "Design of kalman filters for mobile robots; evaluation of the kinematic and odometric approach," in *Proceedings of the 1999 IEEE International Conference on Control Applications*, vol. 2. IEEE, 1999, pp. 1021–1026.

[47] E. Reznick, K. Embry, and R. Gregg, "Predicting individualized joint kinematics over a continuous range of slopes and speeds," in *Int. Conf. Biomedical Robotics Biomechatronics*. IEEE, 2020.

[48] G. Gibson, O. Dosunmu-Ogunbi, Y. Gong, and J. Grizzle, "Terrain-aware foot placement for bipedal locomotion combining model predictive control, virtual constraints, and the alip," *arXiv*, 2021.

[49] B. J. Hafner and J. E. Sanders, "Considerations for development of sensing and monitoring tools to facilitate treatment and care of persons with lower limb loss," *J. rehabilitation research and development*, vol. 51, no. 1, p. 1, 2014.

[50] E. A. Baran, E. Golubovic, and A. Sabanovic, "A new functional observer to estimate velocity, acceleration and disturbance for motion control systems," in *IEEE Int. Symp. Ind. Electron.*, 2010, pp. 384–389.

[51] S.-M. Yang and S.-J. Ke, "Performance evaluation of a velocity observer for accurate velocity estimation of servo motor drives," *IEEE Trans. Industry Applications*, vol. 36, no. 1, pp. 98–104, 2000.

[52] K. Akbari Hamed, B. Safaee, and R. D. Gregg, "Dynamic output controllers for exponential stabilization of periodic orbits for multidomain hybrid models of robotic locomotion," *J. Dynamic Systems, Measurement, and Control*, vol. 141, no. 12, 2019.

Jonathan Horn (S'17) received the B.S. and M.S. degrees in mechanical engineering from Texas A&M University, College Station, TX, USA, in 2013 and 2015, respectively. He received the Ph.D. degree in mechanical engineering at University of Texas at Dallas, Richardson, TX, USA, in 2020. His research interests include nonlinear control, robotic locomotion, hybrid systems, and wearable robotic systems.

Robert D. Gregg (S'08-M'10-SM'16) received the B.S. degree in electrical engineering and computer sciences from the University of California at Berkeley in 2006, and the M.S. and Ph.D. degrees in electrical and computer engineering from the University of Illinois at Urbana-Champaign in 2007 and 2010, respectively. He joined the Department of Electrical Engineering and Computer Science and the Robotics Institute, University of Michigan, as an Associate Professor in 2019. He was previously an Assistant Professor at The University of Texas at Dallas. His research concerns the control of bipedal locomotion and wearable robots.